Lattice-solvent controlled spin transitions in iron(II) complexes†

Chandrasekar Rajadurai, Zhirong Qu, Olaf Fuhr, Balaji Gopalan, Robert Kruk, Mohammed Ghafari and Mario Ruben*

Received 12th March 2007, Accepted 7th June 2007
First published as an Advance Article on the web 9th July 2007
DOI: 10.1039/b703700g

A series of spin transition (ST) iron(II) compounds of the type $[Fe^{II}\mathbf{L}_2](X)_2\cdot\{\mathbf{S}\}_2$ (where **L** is 4′-(4‴-cyanophenyl)-1,2′:6′1″-bispyrazolylpyridine, X = ClO_4^- or BF_4^-, and **S** is acetonitrile) was synthesized and magnetically investigated. The effects of the removal of the lattice-solvent molecules and of their different positions relative to the iron(II) cations on the ST process were investigated. Crystallization yields orange block (**A**·{**S**}$_2$) crystals of the composition $[Fe^{II}(\mathbf{L})_2](ClO_4)_2\cdot\{\mathbf{S}\}_2$, and two polymorphic compounds of the stoichiometry $[Fe^{II}(\mathbf{L})_2](BF_4)_2\cdot\{\mathbf{S}\}_2$ as red coffin (**B**·{**S**}$_2$) and orange block (**C**·{**S**}$_2$) crystals. The Fe–N bond distances of **A**·{**S**}$_2$ (from 1.921(9) to 1.992(3) Å; at 150 K), **B**·{**S**}$_2$ (from 1.943(2) to 2.017(2) Å; at 180 K) and **C**·{**S**}$_2$ (from 1.883(3) to 1.962(3) Å; at 180 K) indicate low spin (LS) states of the respective iron(II) ions. Notably, the observed small difference in the Fe–N distances at 180 K for the two polymorphs **B**·{**S**}$_2$and **C**·{**S**}$_2$ are due to different positions of the acetonitrile molecules in the crystal lattices and illustrate the sensitivity of the spin transition properties on lattice-solvent effects. Variable-temperature single crystal X-ray studies display single-crystal thermochroism (red (LS) ↔ orange (HS)) for **A**·{**S**}$_2$ and **B**·{**S**}$_2$ and *ca.* 3.6% decrease in the unit cell volume of **A**·{**S**}$_2$ from 4403 Å^3 at 300 K to 4278 Å^3 at 150 K. The temperature dependent magnetic susceptibilities of **A**·{**S**}$_2$ and **B**·{**S**}$_2$ demonstrate systematic increase of the spin transition temperatures ($T_{1/2}$) and continuous decreases of the hysteresis loop width ($\Delta T_{1/2}$) upon slow lattice-solvent exclusion.

Introduction

Spin transition (ST) compounds displaying high transition temperatures ($T_{1/2}$), wide thermal hysteresis ($\Delta T_{1/2}$) and thermochroism are increasingly the focus of scientific interest due to their potential applicability in molecular devices.[1–3] It is apparent that the character of a thermal ST compound is strongly influenced by factors such as ligand-field strength, lattice-solvents,[4] counterions[1,5] and polymorphism.[6] These factors determine the propensity of iron(II) complexes towards high-spin (HS) ↔ low-spin (LS) state switching, their abruptness, multistep nature, $T_{1/2}$ and $\Delta T_{1/2}$.

In ST compounds the presence of an intermolecular solid state *cooperative effect* is very important in order to achieve high $\Delta T_{1/2}$ values. In this context, the lattice-solvents play a critical role in spreading the elastic interactions[2e] caused by the Fe–N bond distance changes of *ca.* 0.2 Å. Importantly, the presence or absence of lattice-solvent molecules in a ST compound determines the degree of intermolecular cooperativity in the solid state. Hence the understanding of the function of lattice-solvent molecules in a ST compound is essential in order to tune the ST parameters such as $T_{1/2}$ and $\Delta T_{1/2}$. Despite this fact, only a few systematic studies are dedicated to the investigation of the influence of the lattice-solvents on the critical $T_{1/2}$ and $\Delta T_{1/2}$ parameters of ST–iron(II) compounds. Sometimes, solvate molecules trap or allow spin transition and removal of solvates from the ST compound increases the spin transition temperature but mostly at the expense of the hysteresis loop width.[4]

The goal of this work is to demonstrate that, by manipulating the solvent molecules in crystal lattices of iron(II) complexes, the ST behaviour can be rationally fine-tuned. Herein, we investigate the change in the ST parameters ($T_{1/2}$ and $\Delta T_{1/2}$) of crystalline iron(II) complexes (i) by removing the lattice-solvent molecules from the bulk crystals in a step-wise manner and (ii) by varying the positions of the solvent molecules within the crystal lattice. Towards this goal, we report on the single crystal X-ray investigation of the complexes $[Fe^{II}(\mathbf{L})_2](ClO_4)_2\cdot 2CH_3CN$ (**A**·{**S**}$_2$) and of two polymorphs of $[Fe^{II}(\mathbf{L})_2](BF_4)_2\cdot 2CH_3CN$ (orange (**B**·{**S**}$_2$) and red (**C**·{**S**}$_2$ morphologies), where **L** is (4′-(4‴-cyanophenyl)-1,2′:6′1″-bispyrazolylpyridine). Simultaneously, we study the change of the ST properties of **A**·{**S**}$_2$ and **B**·{**S**}$_2$ upon *in situ* slow removal of the lattice-acetonitrile molecules during the SQUID magnetic measurements by four continuous heating and cooling cycles. Room temperature Fourier Transform Infrared (FTIR) analysis confirms solvate removal thereby supporting the magnetic investigations. Powder X-ray diffraction (XRD) investigations further verify the transformation of the crystal lattices due to the solvate removal.

Experimental

General

4-Cyanophenylboronic acid, $Pd(PPh_3)_4$, $Fe(BF_4)_2$hydrate, and $Fe(ClO_4)_2$hydrate were obtained from Aldrich and used as

Institute of Nanotechnology, Research Centre, Karlsruhe, PB-3640, D-76021, Germany. E-mail: Mario.Ruben@int.fzk.de; Fax: +49 724-782-6781; Tel: +49 724-782-6434

† CCDC reference numbers 634174–634176. For crystallographic data in CIF or other electronic format see DOI: 10.1039/b703700g

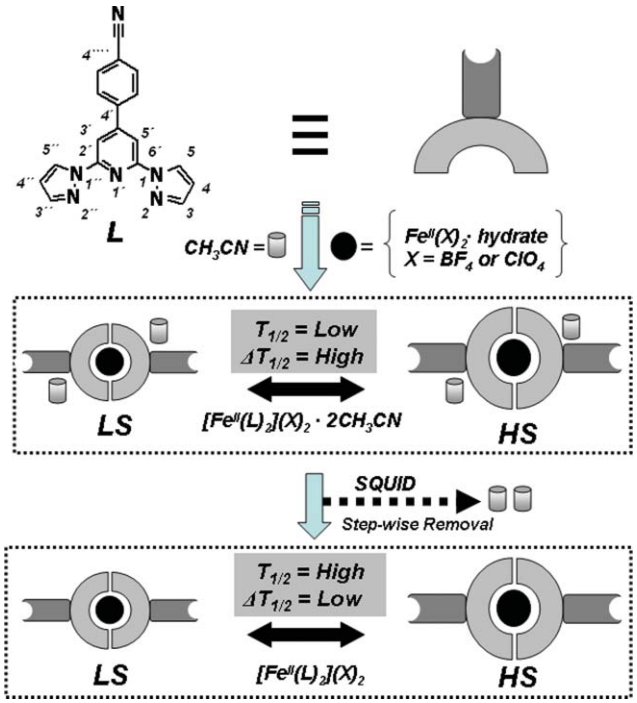

Scheme 1 Representation of the components used in the synthesis of spin transition complexes (**A**·{**S**}$_2$, **B**·{**S**}$_2$ and **C**·{**S**}$_2$) and the investigation of the solvate role in the magnetic properties.

received. Toluene, dichloromethane, diisopropyl ether, acetonitrile and methanol solvents were used without any further purification. ^{1}H and ^{13}C NMR spectroscopic data were recorded on a Bruker DPX 300 spectrometer with solvent proton as the internal standard. Infrared spectra were recorded using KBr pressed pellets on a Perkin Elmer Spectrum GX FT–IR spectrometer. MALDI-TOF MS data were acquired with a Voyager-DE PRO Bio spectrometry work station. Elemental analyses were carried out on a Vario MICRO cube.

Magnetic susceptibility

Temperature and solvate dependent static susceptibilities of complexes **A**·{**S**}$_2$ and **B**·{**S**}$_2$ were recorded for four continuous cooling and heating cycles (2 K min^{-1}) using a MPMS-5S (Quantum Design) SQUID magnetometer over a temperature range of 4.5↔380 K in a homogeneous 0.1 Tesla external magnetic field. Gelatin capsules were used as sample containers for measurements taken in the temperature range of 4.5↔380 K. The very small diamagnetic contribution of the gelatin capsule had a negligible contribution to the overall magnetization, which was dominated by the sample. The diamagnetic corrections of the molar magnetic susceptibilities were applied using well-known Pascal's constants.

Single crystal and powder X-ray diffraction

Single X-ray data collection was performed on a STOE IPDS II diffractometer with graphite monochromated Mo-Kα radiation (0.71073 Å). The structure was solved by direct methods (SHELX-97). Refinement was performed with anisotropic temperature factors for all non-hydrogen atoms. The powder diffraction data of polycrystalline samples were collected by using a Phillips X′Pert diffractometer in Bragg–Brentano geometry with Cu-Kα (1.54184 Å) radiation.

Synthesis of ligand and iron(II) complexes

4-Iodo-2,6-di-pyrazol-1-ylpyridine was synthesized following reported procedures.[7]

4′-(4‴-cyanophenyl)-1,2′:6′1″-bispyrazolylpyridine (L). 4-iodo-2,6-di-pyrazol-1-ylpyridine (0.69 g, 2 mmol) and 4-cyanophenylboronic acid (0.31 g, 2 mmol) was suspended in N_2 bubbled solvents of MeOH–toluene (1 : 1, 100 mL) and 2 M Na_2CO_3 (8 mL). The mixture was heated to 70 °C for 2 d under a nitrogen atmosphere. The crude reaction mixture was poured into ice water (500 mL) and extracted with CH_2Cl_2 solvent. The separated organic layer was dried over $MgSO_4$ and the solvent was removed by evaporation. The solid residue was purified by column chromatography on silica with CH_2Cl_2 as the eluent to obtain compound **L** as a white powder. Yield 0.35 g, 56%. ^{1}H NMR (300 MHz, $CDCl_3$): δ = 8.61 (d, 2H), 8.10 (s, 2H), 7.91 (d, 2H), 7.82 (d, 2H), 7.79 (d, 4H), 6.54 (d, 2H) ppm. ^{13}C NMR (75 MHz, $CDCl_3$, 25 °C): 152.48, 152.27, 143.08, 142.30, 133.27, 128.38, 127.70, 118.69, 113.83, 108.71, 107.74 ppm. FT–IR (KBr): ν/cm^{-1} = 2229 (ms, CN band). MALDI-TOF m/z (relative intensity of isotopic distribution in %): Observed: 312.69 (100%), 313.70 (22%), 314.71 (2%). Simulated: 312.11 (100%), 313.11 (22%), 314.11(2%).

[Fe^{II}(L)$_2$](ClO$_4$)$_2$·2CH$_3$CN (A·{S}$_2$). In a 100 mL Schlenk tube, a solution of **L** (103 mg, 0.33 mmol) and $Fe(ClO_4)_2 \cdot 6H_2O$ (40 mg, 0.15 mmol) in acetonitrile (15 mL) was heated at 80 °C for 6 h. The reaction mixture was cooled to room temperature and 80 mL of diisopropyl ether was added under a N_2 flow at RT to yield an orange–yellow precipitate of the complex **A**·{**S**}$_2$. Orange coloured crystals were grown from diffusing the diisopropyl ether into an acetonitrile solution of the complex under N_2 at RT. Yield *ca.* 65 mg. Elemental analysis calcd for, $C_{40}H_{30}C_{12}FeN_{14}O_8$, C 49.95, H 3.12, N 20.36%. Found: C 48.86, H 2.92, N 19.96%.

Caution. *Although we have experienced no difficulties in handling this compound, metal-organic perchlorates are potentially explosive and should be handled with care in small quantities.*

[Fe^{II}(L)$_2$](BF$_4$)$_2$·2CH$_3$CN (B·{S}$_2$) and (C·{S}$_2$). A similar procedure as for A was applied using $Fe(BF_4)_2 \cdot 6H_2O$ (50 mg, 0.15 mmol). Crystallization yielded two distinctive orange block (**B**·{**S**}$_2$) and red coffin (**C**·{**S**}$_2$) shaped crystalline polymorphs. (Yield *ca.* 50 mg of **B**·{**S**}$_2$). Elemental analysis calcd for, $C_{40}H_{30}B_2FeN_{14}F_8$ (**B**·{**S**}$_2$), C 51.31, H 3.21, N 20.95%. Found: C 50.17, H 3.10, N 20.60%.

Result and discussion

Synthesis of complexes

Ligand **L** (4′-(4‴-cyanophenyl)-1,2′:6′1″-bispyrazolylpyridine) was obtained *via* Suzuki cross-coupling reaction of 4-iodo-2,6-di-pyrazol-1-ylpyridine[7] with 4-cyanophenylboronic acid as a white powder in 56% yield. All complexes were prepared by the reaction of 2 equivalents of **L** with one equivalent of the respective iron(II) salt in acetonitrile at 80 °C. Single crystals of **A**·{**S**}$_2$, **B**·{**S**}$_2$ and **C**·{**S**}$_2$ were obtained quantitatively by

diffusing diisopropyl ether into an acetonitrile solution of the complexes under a N_2 atmosphere at room temperature. After one week, crystallization of complex $[Fe^{II}(\mathbf{L})_2](ClO_4)_2{\cdot}2CH_3CN$ yielded orange block crystals of solvated complex $\mathbf{A}{\cdot}\{\mathbf{S}\}_2$ (Fig. 1). Crystallization of complex $[Fe^{II}(\mathbf{L})_2](BF_4)_2{\cdot}2CH_3CN$ resulted in two solvated polymorphic forms, with a major amount (*ca.* 50 mg) of orange block $\mathbf{B}{\cdot}\{\mathbf{S}\}_2$ and a minor amount of red coffin $\mathbf{C}{\cdot}\{\mathbf{S}\}_2$ morphologies (Fig. 2). These crystals are found to be stable at room temperature without any decomposition. For magnetic analysis the two polymorphs ($\mathbf{B}{\cdot}\{\mathbf{S}\}_2$ and $\mathbf{C}{\cdot}\{\mathbf{S}\}_2$) were carefully separated under a microscope (*vide infra*). Simple inspection of the colours of the two polymorphs gives the first indication that their spin states are different. The colour of the single crystals also changed from orange (HS state) to dark red (LS state) upon cooling from 300 to 150 K for both $\mathbf{A}{\cdot}\{\mathbf{S}\}_2$ and $\mathbf{B}{\cdot}\{\mathbf{S}\}_2$ indicating the ST behaviour of these complexes (see Fig. 3)

X-Ray structure of complex $\mathbf{A}{\cdot}\{\mathbf{S}\}_2$†

Table 1 summarizes the experimental crystallographic data. Selected bond lengths and bond angles are given in Table 2. The molecular structures of the complexes are displayed in Fig. 1 and 2. Single crystal X-ray structure analysis reveals monoclinic *P*2/*c* symmetry of complex $\mathbf{A}{\cdot}\{\mathbf{S}\}_2$ (Fig. 1). Noticeably, complex $\mathbf{A}{\cdot}\{\mathbf{S}\}_2$ contains two non-bonded CH_3CN solvates per one iron(II) complex cation. The asymmetric units in $\mathbf{A}{\cdot}\{\mathbf{S}\}_2$ consist of the $[Fe(\mathbf{L})_2]$ cation, two corresponding ClO_4 anions (one of them disordered), and two CH_3CN molecules. The complex $\mathbf{A}{\cdot}\{\mathbf{S}\}_2$

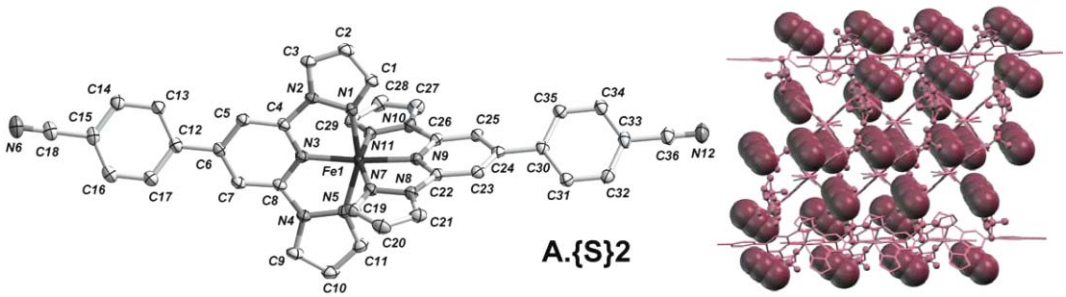

Fig. 1 Left figure: ORTEP view of complex dication in the crystal structures of $[Fe^{II}(\mathbf{L})_2](ClO_4)_2{\cdot}2CH_3CN$ ($\mathbf{A}{\cdot}\{\mathbf{S}\}_2$) (30% probability ellipsoids) unit. Hydrogen atoms, ClO_4 counteranions and lattice-acetonitrile molecules are omitted for clarity. Right figure: crystal packing diagram of complex $\mathbf{A}{\cdot}\{\mathbf{S}\}_2$. H atoms have been removed for clarity. $[Fe^{II}(\mathbf{L})_2]$ dications, counteranions and lattice-acetonitrile molecules are shown in capped sticks, ball and stick and spacefill representations, respectively.

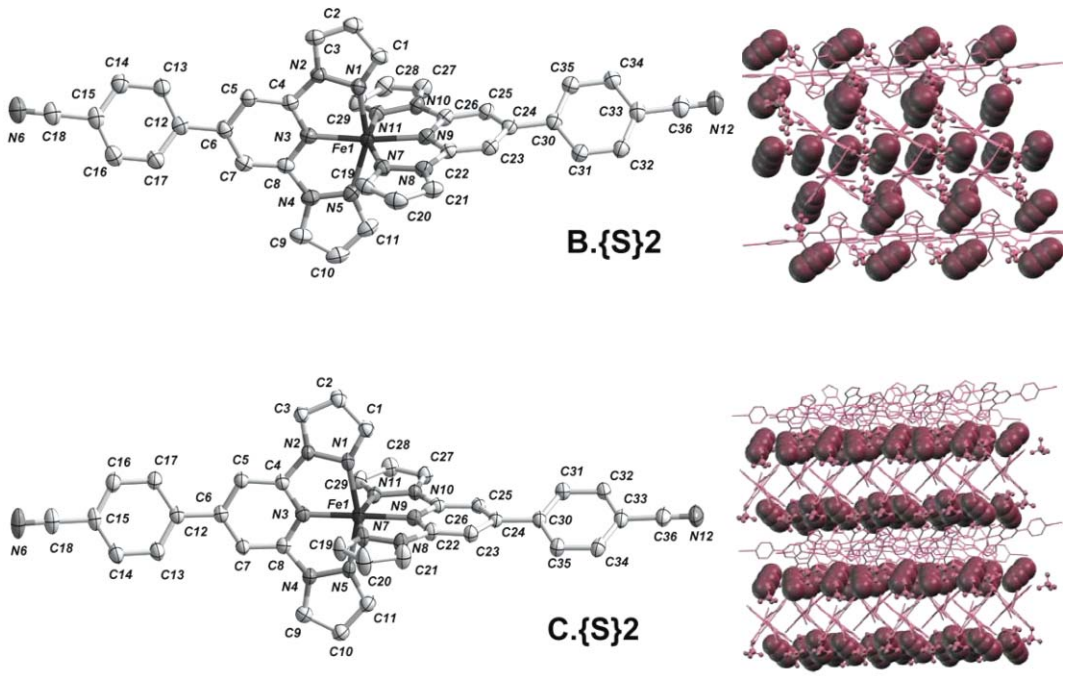

Fig. 2 Left figures: ORTEP view of polymorphs $[Fe^{II}(\mathbf{L})_2](BF_4)_2{\cdot}2CH_3CN$ ($\mathbf{B}{\cdot}\{\mathbf{S}\}_2$) and $[Fe^{II}(\mathbf{L})_2](BF_4)_2{\cdot}2CH_3CN$ ($\mathbf{C}{\cdot}\{\mathbf{S}\}_2$) (30% probability ellipsoids) units. Hydrogen atoms, BF_4 counteranions and lattice-acetonitrile molecules are omitted for clarity. Right figures: crystal packing diagram of $\mathbf{B}{\cdot}\{\mathbf{S}\}_2$ and $\mathbf{C}{\cdot}\{\mathbf{S}\}_2$. $[Fe^{II}(\mathbf{L})_2]$ dications, counteranions and lattice-acetonitrile molecules are shown in capped sticks model, ball and stick and spacefill representations, respectively.

Table 1 Crystallographic parameters of **A**·{**S**}$_2$, **B**·{**S**}$_2$ and **C**·{**S**}$_2$

	$[Fe^{II}(\mathbf{L})_2](ClO_4)_2\cdot 2CH_3CN$	Two polymorphs of $[Fe^{II}(\mathbf{L})_2](BF_4)_2\cdot 2CH_3CN$	
	(**A**·{**S**}$_2$)	(**B**·{**S**}$_2$)	(**C**·{**S**}$_2$)
Formula	$C_{40}H_{30}Cl_2O_8FeN_{14}$	$C_{40}H_{30}B_2F_8FeN_{14}$	$C_{40}H_{30}B_2F_8FeN_{14}$
Formula weight	961.53	936.25	936.25
Crystal colour	Orange	Orange	Red
Temperature/K	150(2)	180(2)	180(2)
Wavelength/Å	0.71073	0.71073	0.71073
Crystal system	Monoclinic	Monoclinic	Orthorhombic
Space group	*P*2/*c*	*P*2/*c*	*Pna*2$_1$
a/Å	10.808(2)	10.691(2)	19.503(4)
b/Å	13.925(3)	13.868(3)	19.129(4)
c/Å	28.685(6)	28.711(6)	11.409(2)
α/°	90	90	90
β/°	97.77	97.64	90
γ/°	90	90	90
V/Å^3	4277.5(15)	4219.2(15)	4256.3(15)
Z, ρ_{calcd}/mg m^{-3}	4, 1.493	4, 1.474	4, 1.461
μ (Mo-K*α*)/mm^{-1}	0.548	0.443	0.439
F(000)	1968	1904	1904
Crystal size/mm	0.48 × 0.27 × 0.15	0.6 × 0.4 × 0.22	0.45 × 0.27 × 0.23
θ range for the data collection/°	1.49 to 25.71	1.43 to 25.71	1.49 to 25.66
Final *R* indices [$I > 2\sigma(I)$]	$R_1 = 0.0375$, $wR_2 = 0.0892$	$R_1 = 0.0564$, $wR_2 = 0.1528$	$R_1 = 0.0514$, $wR_2 = 0.1429$
R indices (all data)	$R_1 = 0.0508$, $wR_2 = 0.0940$	$R_1 = 0.0679$, $wR_2 = 0.1607$	$R_1 = 0.0545$, $wR_2 = 0.1460$
Extinction coefficient	0.00140(19)	0.0178(13)	0.0219(16)
GoF on F^2	1.026	1.013	1.042

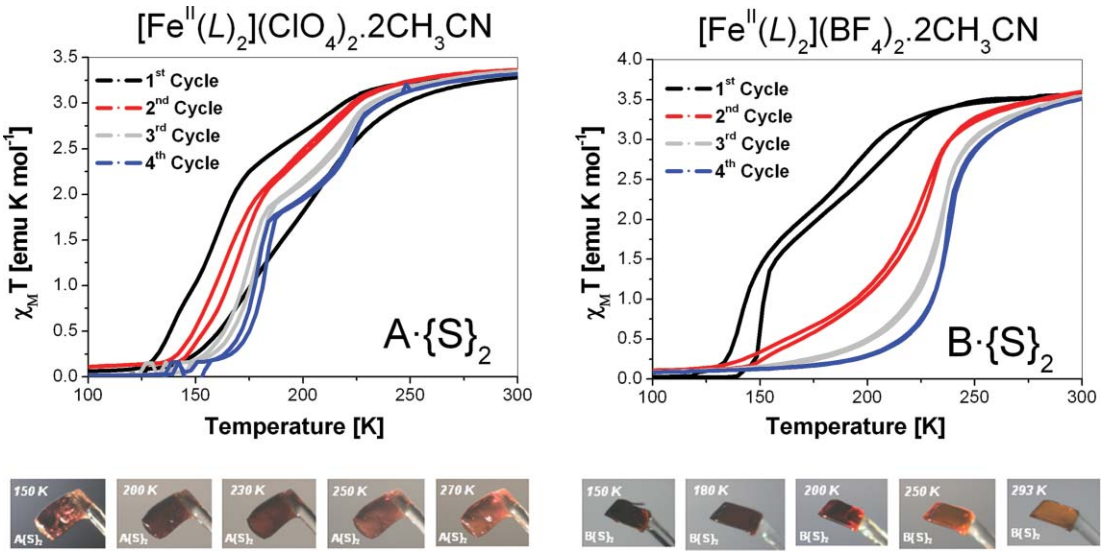

Fig. 3 The χ_M *T vs. T* plot of **A**·{**S**}$_2$ and **B**·{**S**}$_2$ measured in the temperature range of 4.5↔380 K at four continuous cycles (↓ cooling mode and ↑heating mode) with an applied magnetic field of 0.1 T. Bottom photographs show the temperature dependence of the single crystal colour for the acetonitrile solvate of **A**·{**S**}$_2$ and **B**·{**S**}$_2$ (orange and dark red colours correspond to the HS and LS states, respectively).[4b]

shows Fe–N bond lengths ranging from 1.921(9) to 1.992(3) Å at 150 K indicating the LS state of the iron(II) ion. Variable temperature single crystal X-ray studies show a dramatic increase (*ca.* 3.6%) in the unit cell volume with values of 4278, 4305, 4374 and 4403 Å^3 at 150, 200, 250 and 300 K temperatures, respectively.

X-Ray structures of polymorphic complexes B·{S}$_2$ and C·{S}$_2$†

The single-crystal X-ray analysis of the two polymorphs **B**·{**S**}$_2$ and **C**·{**S**}$_2$ reveals monoclinic *P*2/*c* and orthorhombic *Pna*2$_1$ symmetry, respectively (Fig. 2). The asymmetric units in **B**·{**S**}$_2$ and **C**·{**S**}$_2$ consist of the [Fe(**L**)$_2$] cation, two corresponding BF_4 anions, and two CH_3CN molecules. The positions of the acetonitrile molecules within the crystal lattices of **B**·{**S**}$_2$ and **C**·{**S**}$_2$ are different. In the case of **B**·{**S**}$_2$, two acetonitrile molecules are distributed above and below the [Fe(**L**)$_2$] cation core, while in **C**·{**S**}$_2$ they form a continuous 2D layer structure along the crystallographic *ac*-plane (Fig. 2). At 180 K, the two polymorphs show Fe–N bond lengths ranging from 1.943(2) to 2.017(2) Å for **B**·{**S**}$_2$ and from 1.883(3) to 1.962(3) Å for **C**·{**S**}$_2$ which indicate a situation close to the LS state but with more or less an admixture of a residual HS fraction. The slight differences

Table 2 Selected bond distances and angles of $\mathbf{A}\cdot\{\mathbf{S}\}_2$, $\mathbf{B}\cdot\{\mathbf{S}\}_2$ and $\mathbf{C}\cdot\{\mathbf{S}\}_2$

	$\mathbf{A}\cdot\{\mathbf{S}\}_2$	$\mathbf{B}\cdot\{\mathbf{S}\}_2$	$\mathbf{C}\cdot\{\mathbf{S}\}_2$
Temperature/K	150	180	180
Bond distances/Å			
Fe(1)–N(9)	1.924(0)	1.943(2)	1.883(3)
Fe(1)–N(3)	1.921(9)	1.945(2)	1.891(3)
Fe(1)–N(1)	1.971(9)	1.985(2)	1.953(3)
Fe(1)–N(5)	1.992(3)	1.996(2)	1.957(3)
Fe(1)–N(7)	1.984(6)	2.011(3)	1.960(3)
Fe(1)–N(11)	1.988(4)	2.017(2)	1.962(3)
Bond angles/°			
N(9)–Fe(1)–N(3)	174.75(4)	173.47(9)	179.23(12)
N(9)–Fe(1)–N(1)	96.07(8)	96.39(9)	100.37(12)
N(3)–Fe(1)–N(1)	79.40(1)	78.26(9)	80.00(11)
N(9)–Fe(1)–N(5)	105.39(6)	106.71(9)	99.33(11)
N(3)–Fe(1)–N(5)	79.21(1)	78.81(9)	80.29(12)
N(1)–Fe(1)–N(5)	158.46(4)	156.82(9)	160.27(11)
N(9)–Fe(1)–N(7)	79.09(0)	78.30(9)	80.01(11)
N(3)–Fe(1)–N(7)	103.64(0)	105.51(9)	99.32(12)
N(1)–Fe(1)–N(7)	92.63(3)	92.71(9)	91.53(13)
N(5)–Fe(1)–N(7)	89.87(3)	90.15(10)	90.86(13)
N(9)–Fe(1)–N(11)	79.03(0)	78.34(9)	80.08(11)
N(3)–Fe(1)–N(11)	98.42(6)	98.08(9)	100.60(12)
N(1)–Fe(1)–N(11)	92.82(3)	93.32(9)	92.00(12)
N(5)–Fe(1)–N(11)	92.84(3)	93.20(10)	92.40(12)
N(7)–Fe(1)–N(11)	157.88(6)	156.37(9)	160.08(11)

in the Fe–N bond distances in $\mathbf{B}\cdot\{\mathbf{S}\}_2$ and $\mathbf{A}\cdot\{\mathbf{S}\}_2$ at 180 K reveal the influence of different spatial distributions of the same number of solvent molecules within the crystal lattice on the ST properties.

Temperature and solvate dependent magnetic properties of $\mathbf{A}\cdot\{\mathbf{S}\}_2$ and $\mathbf{B}\cdot\{\mathbf{S}\}_2$

The temperature and solvate dependent magnetic susceptibilities of polycrystalline compounds $\mathbf{A}\cdot\{\mathbf{S}\}_2$ and $\mathbf{B}\cdot\{\mathbf{S}\}_2$ were measured at four continuous heating (↑) and cooling (↓) cycles in the temperature range of 380↔4.5 K (Fig. 3).

During the first cycle, the product of the molar magnetic susceptibility and temperature ($\chi_M T$) of compound $\mathbf{A}\cdot\{\mathbf{S}\}_2$ is *ca.* 3.36 emu K mol^{-1} at 380 K, which is close to the value expected for a HS state ($S = 2$) of an iron(II) ion. Upon cooling, the $\chi_M T$ decreases sharply (with two steps) to a value of *ca.* 0.09 emu K mol^{-1} at 125 K, indicating the LS state ($S = 0$) of an iron(II) ion. The first cycle also reveals a broad *ca.* 34 K hysteresis loop with different $T_{1/2}$ values in both cooling ($T_{1/2}\downarrow = 196$ K) and heating ($T_{1/2}\uparrow = 162$ K) mode measurements.

For polymorph $\mathbf{B}\cdot\{\mathbf{S}\}_2$, the first cooling and heating cycle shows a $\chi_M T$ value of *ca.* 3.63 emu K mol^{-1} at 380 K indicating the HS state ($S = 2$) of an iron(II) ion. At 130 K the $\chi_M T$ value sharply decreases to a minimum value of *ca.* 0.03 emu K mol^{-1}, which agrees with the LS state ($S = 0$) of an iron(II) ion. In addition, the first cycle also displays a two step transition centred at *ca.* 150 K with different $T_{1/2}$ values in both cooling ($T_{1/2}\downarrow = 224$ K) and heating ($T_{1/2}\uparrow = 218$ K) mode measurements and a resulting *ca.* 6 K hysteresis loop. It has to be mentioned that the observed discrepancy between the magnetic moment (high spin) and the single crystal X-ray structure (low spin) at the same temperature (180 K) points towards a possible cohabitation of two different species in the bulk of the crystals due to partial solvent removal, which is in agreement with the observation of a two-step transition during the first heating cycle. Unfortunately, due to the poor yield, it was not possible to measure the temperature dependent magnetic susceptibilities of polymorph $\mathbf{C}\cdot\{\mathbf{S}\}_2$. Nevertheless, the average Fe–N bond distance (1.982 Å) obtained from the single-crystal X-ray analysis shows that the compound is close to the LS state at 180 K.

In order to elucidate further the role of the lattice-solvates on the ST properties, the cooling and heating cycle SQUID measurements of the samples $\mathbf{A}\cdot\{\mathbf{S}\}_2$ and $\mathbf{B}\cdot\{\mathbf{S}\}_2$ were continued without interruption (see Table 3). Interestingly, during the 2nd cycle, both complexes displayed increasing $T_{1/2}$ (173 K for $\mathbf{A}\cdot\{\mathbf{S}\}_2$ and 221 K for $\mathbf{B}\cdot\{\mathbf{S}\}_2$) and decreasing $\Delta T_{1/2}$ values (4 K for $\mathbf{A}\cdot\{\mathbf{S}\}_2$ and 2 K for $\mathbf{B}\cdot\{\mathbf{S}\}_2$). Additional 3rd and 4th measurement cycles showed further increasing $T_{1/2}$ values from 181 K to 185 K and from 231 K to 236 K, respectively for $\mathbf{A}\cdot\{\mathbf{S}\}_2$ and $\mathbf{B}\cdot\{\mathbf{S}\}_2$. Moreover, a reduced loop width of only 3 K was observed for $\mathbf{A}\cdot\{\mathbf{S}\}_2$ after the 4th measurement cycle, while the hysteresis loop had completely vanished for $\mathbf{B}\cdot\{\mathbf{S}\}_2$. In addition, a careful look at the evolution of the ST curves of both $\mathbf{A}\cdot\{\mathbf{S}\}_2$ and $\mathbf{B}\cdot\{\mathbf{S}\}_2$ at different cycles reveals striking disparity in their abruptness. In $\mathbf{A}\cdot\{\mathbf{S}\}_2$, a two-step transition is observed during the first cycle, which becomes more pronounced in the subsequent cycles (from 2nd to 4th).[4f] The observed two-step transition boundary was shifted from 173 K to 185 K at the end of the 4th cycle with an emerging abruptness during the 2nd step. While, the ST curve of $\mathbf{B}\cdot\{\mathbf{S}\}_2$ became smoother upon continuous measurement cycles and an abrupt transition was observed only during the 4th cycle. Both complexes $\mathbf{A}\cdot\{\mathbf{S}\}_2$ and $\mathbf{B}\cdot\{\mathbf{S}\}_2$ display no change in the magnetic behaviour beyond the 4th cycle. This is interpreted in terms of complete removal of solvates from the crystal lattice.

Powder XRD data

The phase structures of the isocrystallographic complexes $\mathbf{A}\cdot\{\mathbf{S}\}_2$ and $\mathbf{B}\cdot\{\mathbf{S}\}_2$ before and after SQUID magnetic measurement cycles were examined by powder X-ray diffraction (XRD) studies at 293 K. The XRD pattern of $\mathbf{A}\cdot\{\mathbf{S}\}_2$ and $\mathbf{B}\cdot\{\mathbf{S}\}_2$ are given in Fig. 4. Noticeably, the single crystal XRD studies performed on a fresh crystal of $\mathbf{A}\cdot\{\mathbf{S}\}_2$ show that the crystal system (monoclinic, $P2/c$) remains unchanged during the cooling mode measurements from

Table 3 Spin transition temperatures ($T_{1/2}$) and hysteresis loop widths ($\Delta T_{1/2}$) of complexes $\mathbf{A}\cdot\{\mathbf{S}\}_2$ and $\mathbf{B}\cdot\{\mathbf{S}\}_2$ measured during four continuous cooling (↓) and heating (↑) cycles

	$[Fe^{II}(\mathbf{L})_2](ClO_4)_2\cdot 2CH_3CN$ $\mathbf{A}\cdot\{\mathbf{S}\}_2$				$[Fe^{II}(\mathbf{L})_2](BF_4)_2\cdot 2CH_3CN$ $\mathbf{B}\cdot\{\mathbf{S}\}_2$			
Cycles(↓↑)	1	2	3	4	1	2	3	4
$T_{1/2}$/K	179	173	181	185	166	221	231	236
$\Delta T_{1/2}$/K	34	4	4	3	6	2	0	0

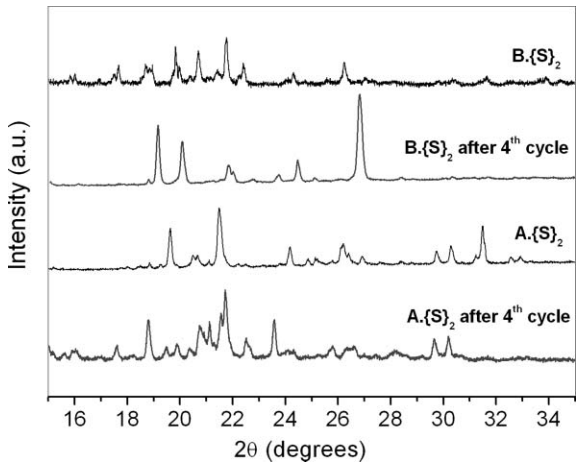

Fig. 4 Room temperature powder XRD data of **A**·{**S**}$_2$ and **B**·{**S**}$_2$ before and after the four cooling and heating cycles.

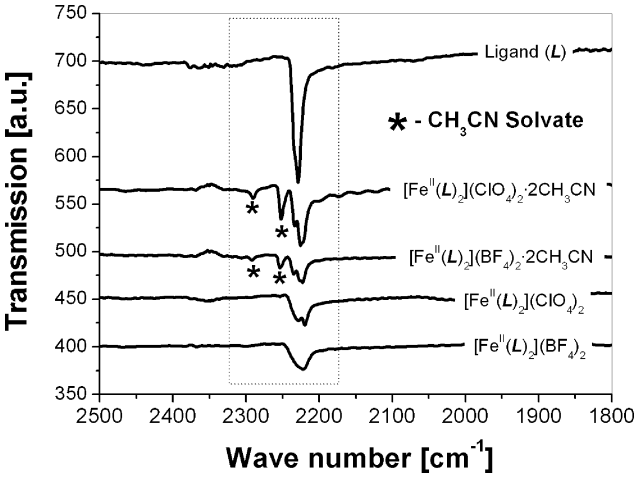

Fig. 5 FTIR spectra (2500–1800 cm^{-1} region) of KBr pelleted complexes (**A**·{**S**}$_2$ and **B**·{**S**}$_2$) before 1st and after the 4th cooling and heating cycles. The spectra of ligand **L** is shown for comparison. * show the –C≡N stretching frequencies from the lattice-acetonitrile.[8]

293 K to 150 K ruling out the possibility of any phase transition in the single crystal XRD measurements conditions. Both powdered samples of **A**·{**S**}$_2$ and **B**·{**S**}$_2$ show slightly different peak patterns apparently as a result of slow solvent loss during the room temperature powder XRD data collection conditions (see Fig. 4).

The comparison of the room temperature powder XRD data of **A**·{**S**}$_2$ and **B**·{**S**}$_2$ with the corresponding calculated low spin powder XRD data (180 K) reveals completely different patterns. These results support the fact that the spin transition behaviours observed during the 1st heating cycle (under a SQUID environment) in both **A**·{**S**}$_2$ and **B**·{**S**}$_2$ are accompanied by phase transitions. This is also in accordance with the observation of two-step spin transitions for **A**·{**S**}$_2$ and **B**·{**S**}$_2$ during the magnetic measurements. To explore further alteration of the crystal structure due to solvate desorption, the powder XRD patterns before the 1st measurement cycle and after the 4th measurement cycle were collected and compared. As expected complexes **A**·{**S**}$_2$ and **B**·{**S**}$_2$ show absolutely different patterns before and after the SQUID measurements, which ascertain that the final structural change is caused by step-wise desorption of lattice-acetonitrile molecules from the crystals. In addition, the initially isocrystallographic compounds **A**·{**S**}$_2$ and **B**·{**S**}$_2$ develop into two different diffraction patterns after the 4th magnetic cycle due to solvate removal. This observation is clearly in agreement with the observation of different magnetic behaviours observed during the 4th magnetic cycle for both compounds.

FTIR spectra of complexes

In order to further confirm the entire solvate removal from the polycrystalline samples, room temperature FTIR measurements for **A**·{**S**}$_2$ and **B**·{**S**}$_2$ were performed before and after magnetic measurements (Fig. 5). The cyano functional group of the ligand **L** shows a low frequency $\nu_{C\equiv N}$ stretching band centred at 2229 cm^{-1}. Before the SQUID measurement, both complexes **A**·{**S**}$_2$ and **B**·{**S**}$_2$ show characteristic $\nu_{C\equiv N}$ stretching frequencies bands centred at 2223 and 2234 cm^{-1}for the cyano groups of the coordinated ligands. Additionally, complexes **A**·{**S**}$_2$ and **B**·{**S**}$_2$ show distinctive low (2251 and 2254 cm^{-1}) and high frequency (2291 and 2292 cm^{-1}) bands for the lattice-acetonitrile molecules. The frequency separation of *ca.* 40 cm^{-1}and the typical intensities of the lower and higher frequency bands further confirms the solvate band assignment.[8] Noticeably, both complexes show absolute disappearance of the two characteristic acetonitrile $\nu_{C\equiv N}$ stretching bands after the completion of the fourth magnetic measurement cycle (see * in Fig. 5). This result unequivocally confirms the slow removal of lattice-acetonitrile molecules from the crystalline samples during the continuous magnetic measurement cycles and their complete removal at the end of fourth cycle.

The observed increase in $T_{1/2}$ and decrease in $\Delta T_{1/2}$ in strong dependence of the number of heating/cooling cycles can be attributed to the diminution of solvate assisted cooperativity between the ST centres due to the slow solvate removal.[4] In-depth Mössbauer investigations are in progress at different heating and cooling and cycles in the temperature range of 5–380 K to investigate the cooperativity associated with the slow solvent removal and also the relaxation dynamics of the complexes.

Conclusions

In conclusion, the results presented here illustrate the effect of the removal of lattice-solvent molecules and of their relative positions within the crystal-lattice on the magnetic spin states of the iron(II) ion, in particular on the ST parameters ($T_{1/2}$ and $\Delta T_{1/2}$). Despite the complexity of the considered three molecular systems **A**·{**S**}$_2$, **B**·{**S**}$_2$, and **C**·{**S**}$_2$ exhibiting a high degree of freedom in the positions of the anions and solvent molecules so leading to different polymorphs, this study proves that the control of the lattice-solvent molecules can be used rationally to achieve technologically attractive spin transition temperatures.

Acknowledgements

The authors thank the Deutsche Forschungsgemeinschaft (DFG) for financial support within the frame of the project "Kondo Molecules". We thank Prof. Dr Horst Hahn for providing instrument facilities and the referees for constructive comments.

References

1 For general reviews: (*a*) *Spin Crossover in Transition Metal Compounds I, Topics in Current Chemistry*, ed. P. Gütlich and H. A. Goodwin, Springer, Berlin, 2004, vol. 233; (*b*) H. Spiering, *Spin Crossover in Transition Metal Compounds III, Topics in Current Chemistry*, Springer-Verlag, Berlin, 2004, vol. 235, p. 171 and references therein; (*c*) P. Gütlich, *Struct. Bonding*, 1981, 83–195; (*d*) P. Gütlich and A. Hauser, *Coord. Chem. Rev.*, 1990, **97**, 1–22; (*e*) E. König, *Prog. Inorg. Chem.*, 1987, **35**, 527–623; (*f*) J. A. Real, A. B. Gaspar, V. Niel and M. C. Muñoz, *Coord. Chem. Rev.*, 2003, **236**, 121; (*g*) A. B. Gaspar, V. Ksenofontov, M. Seredyuk and P. Gütlich, *Coord. Chem. Rev.*, 2005, **249**, 2661; (*h*) P. Gütlich, Y. Garcia and T. Woike, *Coord. Chem. Rev.*, 2001, **839**, 219–221; (*i*) P. Gütlich, A. Hauser and H. Spiering, *Angew. Chem., Int. Ed. Engl.*, 1994, **33**, 2024–2054; (*j*) M. A. Halcrow, *Coord. Chem. Rev.*, 2005, **249**, 2880.

2 (*a*) O. Kahn and C. Jay Martinez, *Science*, 1998, **279**, 44; (*b*) J. A. Real, E. Andres, M. C. Muñoz, M. Julve, T. Granier, A. Bousseksou and F. Varret, *Science*, 1995, **268**, 265–267; (*c*) O. Kahn, J. Kröber and C. Jay, *Adv. Mater.*, 1992, **4**, 718; (*d*) A. Galet, A. B. Gaspar, M. C. Muñoz, G. V. Bukin, G. Levchenko and J. A. Real, *Adv. Mater.*, 2005, **17**, 2949–2953; (*e*) I. Sanner, E. Meissner, H. Köppen and H. Spiering, *Chem. Phys.*, 1984, **86**, 227.

3 (*a*) M. Ruben, F. J. Rojo, J. Romero-Salguero and J.-M. Lehn, *Angew. Chem., Int. Ed.*, 2004, **43**, 3644–3662; (*b*) M. Ruben, U. Ziener, J.-M. Lehn, V. Ksenofontov, P. Gütlich and G. B. M. Vaughan, *Chem.–Eur. J.*, 2005, **11**, 94–100; (*c*) M. Ruben, E. Breuning, J.-M. Lehn, V. Ksenofontov, F. Renz, P. Gütlich and G. B. M. Vaughan, *Chem.–Eur. J.*, 2003, **9**, 4422–4429; (*d*) E. Breuning, M. Ruben, J.-M. Lehn, F. Renz, Y. Garcia, V. Ksenofontov, P. Gütlich, E. Wegelius and K. Rissanen, *Angew. Chem., Int. Ed.*, 2000, **39**, 2504–2507.

4 (*a*) A. Galet, M. C. Muñoz and J. A. Real, *Chem. Commun.*, 2006, 4321–4323; (*b*) V. Niel, A. L. Thompson, M. C. Muñoz, A. Galet, A. E. Goeta and J. A. Real, *Angew. Chem., Int. Ed.*, 2003, **42**, 3760–3763; (*c*) Y. Garcia, P. J. van Koningsbruggen, R. Lapouyade, L. Fournés, L. Rabardel, O. Kahn, V. Ksenofontov, G. Levchenko and P. Gütlich, *Chem. Mater.*, 1998, **10**, 2426–2433; (*d*) M. Hostettler, K. W. Törnroos, D. Chernyshov, B. Vangdal and N. B. Bürgi, *Angew. Chem., Int. Ed.*, 2004, **43**, 4589–4594; (*e*) S. M. Neville, B. Moubaraki, K. S. Murray and C. J. Kepert, *Angew. Chem., Int. Ed.*, 2007, **46**, 1–5; (*f*) G. J. Halder, C. J. Kepert, B. Moubaraki, K. S. Murray and J. D. Cashion, *Science*, 2002, **298**, 1762.

5 M. Yamada, H. Hagiwara, H. Torigoe, N. Matsumoto, M. Kojima, F. Dahan, J.-P. Tuchagues, N. Re and S. Iijima, *Chem.–Eur. J.*, 2006, **12**, 4536–4549.

6 (*a*) A. Galet, A. B. Gasper, M. C. Muñoz, J. A. Real, G. Levchenko and J. A. Real, *Inorg. Chem.*, 2006, **45**, 9670–9679; (*b*) A. L. Thompson, A. E. Goeta, J. A. Real, A. Galet and M. C. Muñoz, *Chem. Commun.*, 2004, 1390; (*c*) D. L. Reger, J. R. Gardinier, M. D. Smith, A. M. Shahin, G. J. Long, L. Rebbouh and F. Grandjean, *Inorg. Chem.*, 2005, **44**, 1852–1866.

7 (*a*) C. Rajadurai, F. Schramm, S. Brink, O. Fuhr, R. Kruk, M. Ghafari and M. Ruben, *Inorg. Chem.*, 2006, **45**, 10019–10021; see also the ESI; (*b*) C. Rajadurai, O. Fuhr, R. Kruk, M. Ghafari, H. Hahn and M. Ruben, *Chem. Commun.*, 2007, 2636.

8 R. A. Nyquist, *Appl. Spectrosc.*, 1990, **44**, 1405–1407.